A DFT Study on Peroxo-Complex in Titanosilicate Catalyst: Hydrogen Peroxide Activation on Titanosilicalite-1 Catalyst and Reaction Mechanisms for Catalytic Olefin Epoxidation and for Hydroxylamine Formation from Ammonia

Hiroaki Munakata,* Yasunori Oumi, and Akira Miyamoto

Department of Materials Chemistry, Graduate School of Engineering, Tohoku University, Aoba-yama 07, Sendai 980-8579, Japan

Received: June 20, 2000; In Final Form: February 6, 2001

Density functional theory calculations were performed on an activation of hydrogen peroxide over a cluster model of a titanosilicate catalyst. The calculation results showed possibility to form the hydrated peroxo-titanosilicalite complex, containing a (Ti)-O-O-(Si) peroxo-moiety, as an oxidizing agent. Using this hydrated peroxo-titanosilicalite complex as an oxidizing agent, oxidation mechanisms were postulated for ethene epoxidation and for ammonia oxidation to form hydroxylamine. The ethene molecule was oxidized with the peroxo-oxygen coordinated to the central Ti atom of the hydrated peroxo-titanosilicalite complex, to form ethylene epoxide. For the ammonia oxidation process, ammonia replaced the adsorbed water molecule of the hydrated peroxo-titanosilicalite complex. The oxidation of the adsorbed ammonia in the (ammonia)-peroxo-titanosilicalite complex led to the formation of an ammonia-*N*-oxide complex of the titanosilicalite catalyst model. The (ammonia-*N*-oxide)-titanosilicalite complex was transformed into the (hydroxylamine)-titanosilicalite complex, with a hydrogen transfer from the nitrogen to the oxygen of the ammonia-*N*-oxide moiety. The transition states were explored for these reaction processes. Using the peroxo-titanosilicalite complex containing a Ti−O-O-Si peroxo-moiety as an active oxidizing agent, the catalytic reaction mechanisms are proposed for ethene epoxidation and for ammonia oxidation to form hydroxylamine.

Introduction

The isomorphous substitution of Si with Ti into the framework of siliceous microporous and mesoporous solid materials has been extensively explored.[1,2] Zeolite, ZSM-5, is a microporous aluminosilicate, with a pore size of ca. 5.5 Å, and the silicalite analogue of the ZSM-5 structure is denoted as MFI.[3] The Ti-containing MFI-type silicalite (named TS-1) was first prepared by a hydrothermal synthesis at Enichem (Italy).[4] Since then, a large number of Ti-containing siliceous microporous and mesoporous solid materials has been synthesized, e.g., TS-1,[4,5] TS-2,[6] Ti−MCM-48,[7] Ti−β,[8,9], Ti−MCM-12,[10] and Ti−MCM-41.[11,12] These Ti-containing porous silicates exhibited excellent catalytic activities in the oxidation of various organic compounds in the presence of hydrogen peroxide under mild conditions. Catalytic reactions include epoxidation of alkenes,[13−17] oxidation of alkanes,[18] alcohols,[19] amines,[20] hydroxylation of aromatics,[21] and ammoximation of ketones.[22−26] Intensive studies have been carried out on the characterization of titanosilicate catalysts, using X-ray diffraction, IR, Raman, UV−vis spectroscopy and EXAFS.[27−36] Several theoretical studies on the reaction mechanisms for alkene epoxidation over the TS-1 catalyst in the presence of hydrogen peroxide have been reported.[37−42] For alkene epoxidation over the TS-1 catalyst with hydrogen peroxide, a five-membered ring structure, shown in Figure 1a, was speculated and was proposed as a reaction intermediate.[15−17] Neurock et al.[38] performed theoretical studies on a cluster model of the five-membered ring structure for the active Ti-site in the TS-1 catalyst and showed that the ethene interaction with the oxygen O(2) of the terminal OH, was repulsive and that the ethene attack at the oxygen O(1) coordinated to the central titanium was attractive, which led to formation of the epoxide. Vayssilov et al.[39] proposed that hydrogen peroxide was adsorbed nondissociatively with the hydrogen peroxide O−H bond on the cluster model of the TS-1 catalyst. The ethene attack at the oxygen Ob, as shown in Figure 1b, led to formation of the epoxide, with an energy barrier of 83 kJ mol^{-1}, corresponding to the transition state, with respect to the energy of the initial separate reactants at the GGA/BP level of the theory. Sinclair et al.[41] presented the Ti−(η_2-OOR′)(ROH) complex, where R represents ≡SiO−, H, or an organic function, as an active oxygen-donating species in the ethene epoxidation over Ti−silicate catalysts, as shown in Figure 1c. The Ti−(η_2-OOR′)(ROH) complex was derived from the $[(SiO-)_3Ti(-OR)\cdots R'OOH]_{ads}$ complex, and the ethene interacted with the active peroxide oxygen coordinated to the Ti^{IV} center, to give the epoxide with an activation barrier of around

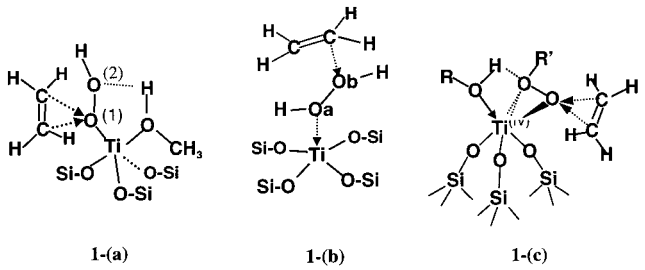

Figure 1. TS-1 active site models with an ethene attacking site. (a) Five-membered active site model, (b) ethene epoxidation with a hydrogen peroxide nondissociatively adsorbed on TS-1 cluster model, (c) Ti−(η_2-OOR′)(ROH) complex model.

* To whom correspondence should be addressed. E-mail: hirom@aki.che.tohoku.ac.jp.

10.1021/jp0022196 CCC: $20.00
Published on Web 04/04/2001

70 kJ mol^{-1} using BP86 functional and DZVP basis. A number of reaction mechanisms and active oxidizing intermediates in the ethene epoxidation process over Ti−silicate catalysts have been presented and are still in debate.

The ammoximation of cyclohexanone over titanosilicalite catalysts in the presence of ammonia and hydrogen peroxide led to the production of cyclohexanone oxime, which is an industrially important raw material for Nylon-6 production. Several studies on reaction mechanisms for the ammoximation of ketones have been reported. Among them, two reaction pathways have been proposed: (1) to proceed through the oxidation of the intermediate of an unstable ketoimine,[23,27] and (2) to proceed via the formation of hydroxylamine from ammonia; the produced hydroxylamine then successively reacted with ketones to produce the corresponding oximes.[24,26] The experimental results showed that the titanosilicalite-1 (TS-1) catalyst performed high activity in the ammoximation of bulky ketones which were hardly diffusing in the pores.[24] In the absence of a ketone, hydroxylamine was produced from ammonia over the TS-1 catalyst in the presence of hydrogen peroxide.[25] Wu et al. reported the ammoximation of ketones over a titanium mordenite catalyst in the presence of hydrogen peroxide and discussed the reaction mechanisms.[26] There were experimental results which showed the formation of the ketoimine over TS-1 and Ti−mordenite catalysts, but the unstable ketoimine decomposed in the presence of a large amount of water to reproduce the starting material of the ketone. Kinetic studies were carried out on the hydroxylamine formation over the titanium-mordenite catalyst in the presence of ammonia, hydrogen peroxide, and ketones, and successive formations of the ketone oximes from various ketones with different reaction rates were observed. On the basis of these experimental results, the reaction pathway via the hydroxylamine formation was proposed. Theoretical quantum chemical calculations have not been performed on the reaction mechanisms for the hydroxylamine formation over the TS-1 catalyst in the presence of ammonia and hydrogen peroxide.

In this work, density functional theory (DFT) calculations were performed on the activation of hydrogen peroxide on the cluster model of the titanosilicalite-1 (TS-1) catalyst. In the course of current studies, possibility to form the peroxo-TS-1 complex, containing a Ti-O-O-Si moiety, was revealed. Using this peroxo-TS-1 complex as an oxidizing agent, the postulated reaction mechanisms for the catalytic ethylene epoxidation and for the hydroxylamine formation from ammonia were investigated.

Materials and Methods

All density functional theory (DFT) calculations were carried out by the DMol, ver. 290, program.[43] The atomic orbital basis sets used throughout were the standard DMol double numerical atomic basis sets augmented with polarization functions (DNP) obtained from exact numerical LDA calculations on the constituent atoms and cationic states of these atoms. Additionally, only the molecular orbital (MO) coefficients corresponding to valence orbitals were included in the self-consistent field (SCF) procedure. Thus, the MO coefficients corresponding to the core orbitals of, Si-, O-, N-, C-1s, and Ti-1s2s2p were fixed at the atomic values in the molecular SCF procedure. Optimizations of molecular geometries and transition state searches were done using the EF algorithm and the mode following method, as implemented in DMol by Baker et al.[44,45] For locating transition states, a quasi-Newton algorithm is used, where attempts are made to maximize along the mode with the negative Hessian eigenvalue and minimize along the modes with positive Hessian eigenvalues. The transition-state structures had a single, negative Hessian eigenvalue. Optimization was done until the change in the value of the maximum gradient was less than 0.003 atomic units. The SCF convergence criterion was less than 2×10^{-6} atomic units. The local density approximation (LDA) with the Vosko-Wilk-Nusair local functional (VWN) was applied to optimize geometries. Energies were calculated on the LDA optimized geometries at a generalized gradient approximation (GGA) with the Becke's exchange functional[46] and the Perdew and Wang correlation functional[47] (denoted as BP). In the next section, we validated these calculational conditions by comparing the results obtained from different calculation schemes. In the following sections, all geometrical parameters are obtained from LDA optimization, unless otherwise stated, and all energetic properties are evaluated using GGA/BP calculation. In the present study, the comparative order of the relative reaction energies of the reactant interacted catalyst model system is more important.

Reaction Energies (E_{react}) were calculated using the following equation: $E_{react} = \sum E_{product} - \sum E_{reactant}$, where E_{react}, $E_{product}$, and $E_{reactant}$ represent the binding energies of the corresponding reaction, a product and a reactant, respectively. The negative E_{react} values mean that the product states are energetically favorable.

InsightII[48] and WebLabViewerLite[49] were used for the graphics display and analysis.

Calculation Models

Cluster Model for Titanium Site. A Si atom at a crystallographic T-site (tetraheral coordination site for Si or Ti) of the orthorhombic MFI-type silicalite crystal was substituted with a Ti atom. The cluster model was constructed by extracting the Ti atom from the Ti-substituted MFI-type silicalite crystal together with the nearest-neighbor four SiO_4 groups. Hydrogen was added to the dangling bond of the terminal oxygen along the bonding direction to the adjacent Si atom, to give the cluster model of $Ti[-O-Si(OH)_3]_4$. The cluster models were constructed for the Ti-substituted T1-, T6-, T8-, and T12-sites of the MFI-type silicalite crystal of the TS-1 catalyst. These T-sites were selected based on published reports.[39,50−52] The positions of the modeled T-sites in the MFI-type silicalite crystal are shown in Figure 2. All of these T-site cluster models have the same chemical formula of $TiSi_4O_{16}H_{12}$. To simulate the local part of the crystal structure, all terminal hydrogen atoms of the cluster model were fixed at the initial coordinates throughout the calculations in this study.

To verify the current chosen calculational scheme, the geometric parameters and bonding energies of H_2O and HOOH, obtained using two calculation schemes, were examined, and geometric parameters were compared to the experimental values.[53] Reaction energies for the ethene epoxidaton obtained using two calculation schemes were compared to the experimental values. Geometric parameters and bonding energies of the cluster models for the Ti-site of the TS-1 catalyst were obtained using two calculation schemes, and geometric parameters were compared to the experimental values. Two series of calculations were performed: (i) full geometry optimization at the LDA level, followed by GGA energy calculation and (ii) full geometry optimization at the GGA level. For the cluster model calculation, all terminal hydrogen atoms of the cluster model were fixed at the initial coordinates throughout geometry optimization. The geometric parameters of H_2O and HOOH at LDA optimization and at full GGA optimization are compared

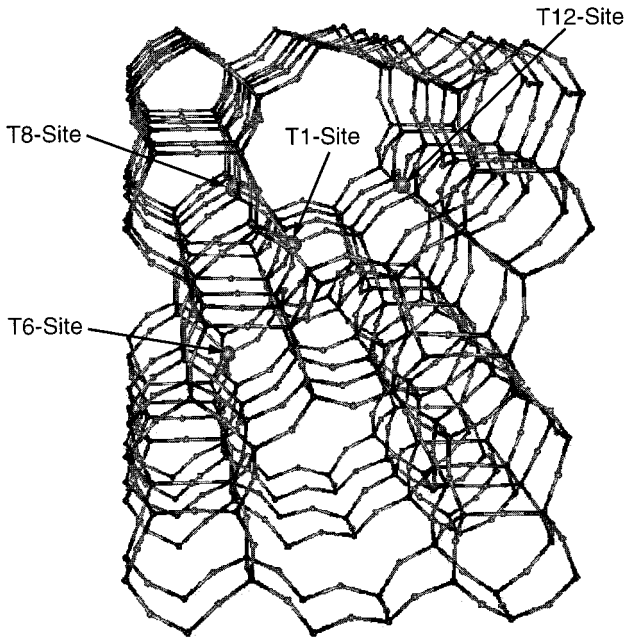

Figure 2. Locations of T-site (tetrahedrally coordinated Ti site) models in the MFI-type silicalite crystal.

TABLE 1: Comparison of the Geometric Parameters of H_2O at LDA + GGA and Full GGA Levels

	rO−H (pm)	aH−O−H (deg)
LDA optimization	98.4	103.7
GGA optimization	98.8	100.5
exp.[53]	95.8	104.5

TABLE 2: Comparison of the Geometric Parameters of HOOH at LDA + GGA and Full GGA Levels

	rO−H (pm)	rO−O (pm)	aO−O−H (deg)
LDA optimization	99.1	145	100
GGA optimization	99.6	152	97
exp.[53]	97 ± 1	149 ± 1	100 ± 2

in Tables 1 and 2. As shown in Tables 1 and 2, the rO−H bond lengths obtained by two schemes gave 2−3 pm longer values compared to the experimental values. The rO−H value at the LDA level was almost the same compared to the value at the full GGA level. The rO−O value at the LDA level is 4 pm shorter and the rO−O value at the full GGA level is 3 pm longer compared to the experimental value, as shown in Table 2. The bond angle aH−O−O of HOOH at the LDA level showed the same value of 100° compared to the experimental value and that of HOOH at the full GGA level showed 3° smaller.

The binding energies for HOOH, ethene, ethylene epoxide and H_2O with LDA optimization followed by GGA energy calculation and with full GGA optimization are presented in Table 3. The binding energies for each compound showed nearly the same values by the two calculation schemes. The epoxidation energy gave the same value of −49 kcal mol^{-1} calculated from these binding energies with both calculation schemes. The value is close to −50.3 kcal mol^{-1} as calculated from standard enthalpies of formation of the reactants and products.[54]

For the Ti-substituted T-site models, the binding energies obtained for the LDA optimization followed by GGA/BP energy calculation and for the full GGA optimization are presented in Table 4. The ranges of bond lengths for Ti−O and Si−O with LDA optimization and with GGA optimization are given together in Table 4. The rTi−O bond lengths at the LDA level are in the range of 178−184 pm which are close to the experimental values, whereas the rTi−O bond lengths at the GGA level are in the range of 181−187 pm. The estimated rTi−O distance was 179 pm based on XRD,[29] and the averaged value of the rTi−O distances was 180−181 ± 1 pm obtained by EXAFS.[30−32] The rSi−O bond lengths at the LDA level are in the range of 165−168 pm which are 4−7 pm longer compared to the experimental values, whereas the rSi−O at the GGA level are 7−12 pm longer compared to the experimental values. The experimetal averaged value of 161 pm was observed for Si−OSi bond length in the X-ray structure of $Cy_7Si_7O_9(OH)_3$, (Cy = cyclohexyl).[33] The estimated rSi−O averaged distance of 159(1) pm was observed in the X-ray structure of ZSM-5.[55] The energy differences between the binding energies for the cluster models at LDA optimization followed by GGA energy calculation and those at full GGA calculation were less than 2.2 kcal/mol. The calculation scheme (i) gave better geometrical parameters compared to those obtained by the calculation scheme (ii). On the basis of these results, we have chosen the calculation condition, that is, the LDA level approximation for geometry optimization followed by GGA energy calculation and a basis set choice, to investigate the TS-1 catalytic reaction system. The binding energies of the Ti-substituted T1, T6, and T12 site models differ less than 3.5 kcal mol^{-1}. The Ti-substituted T8-site model showed the higher relative energy of 11.3 kcal mol^{-1} referred to T1-site model. The Ti-substituted T1-site model of TS-1, indicated as TS-1-Relax **1**, $TiSi_4O_{16}H_{12}$, was adopted to investigate the reaction mechanisms throughout calculations in this study. The choice of the T1-site model was rather arbitrary, since the energy differences among T1, T6, and T12 site models were small.

Results and Discussion

Activation of Hydrogen Peroxide over the TS-1 Catalyst Cluster Model. Interactions of water and hydrogen peroxide with the cluster model **1**, TS-1-Relax, were examined. Energies for the TS-1-(H_2O)-adduct **2** and for TS-1-(HOOH)-adduct **3** relative to the energy of the separate reactants are shown in Table 5. The H_2O adsorption energy was −41 kJ mol^{-1} and the HOOH adsorption energy was −31 kJ mol^{-1}. Activation of hydrogen peroxide over the TS-1 catalyst model was investigated. Results showed that possibility to form the hydrated peroxo-TS-1 complex **7** was revealed, according to the reaction mechanisms postulated in Schemes 1 and 2.

TABLE 3: Comparison of Binding Energies of HOOH, $H_2C{=}CH_2$, Epoxide, and H_2O and the Reaction Energies of the Ethene Epoxidation at LDA + GGA and Full GGA Levels

	binding energies				
	HOOH (kcal/mol)	$H_2C{=}CH_2$ (kcal/mol)	epoxide[a] (kcal/mol)	H_2O (kcal/mol)	E_{react} (kcal/mol)
LDA optimization	−281.8	−560.2	−659.6	−231.2	−48.8
GGA optimization	−281.5	−560.3	−659.6	−231.1	−48.9
reaction energy calculated from the thermodynamic data (CRC)[51]					−50.3

[a] Epoxide = ethylene epoxide.

TABLE 4: Comparison of Binding Energies and Geometrical Parameters of Ti−Substituted T-Site Cluster Models Obtained at LDA + GGA and Full GGA Levels[a]

	T1-site	T6-site	T8-site	T12-site
LDA Optimization + GGA Energy Calculation				
binding E (kcal mol^{-1})	−3524.3	−3520.8	−3513.0	−3522.7
relative E (kcal mol^{-1})	(0.0)	(3.5)	(11.3)	(1.6)
bond length (pm)				
rTi−O	178−183	180−184	179−181	179−183
rSi−O	165−168	165−168	165−167	166−168
GGA Optimization and Energy Calculation				
binding E (kcal mol^{-1})	−3522.9	−3519.3	−3510.8	−3522.3
relative E (kcal mol^{-1})	(0.0)	(3.6)	(12.1)	(0.6)
bond length (pm)				
rTi−O	181−187	184−187	183−185	183−186
rSi−O	168−173	168−173	168−173	169−173

[a] The estimated Ti−O distance was 179 pm based on XRD[29] and the averaged Ti−O distance was 180−181 ± 1 pm obtained by EXAFS.[30−32] The averaged Si−OSi bond length was 161 pm observed in the X-ray structure of $Cy_7Si_7O_9(OH)_3$, (Cy = cyclohexyl)[33] and the estimated Si−O distance was159 (1) pm observed in the X-ray structure of ZSM5.[32]

TABLE 5: Relative Adsorption Energies of Water, Hydrogen Peroxide, and Ammonia on the TS-1 Cluster Model

system for adsorption	LDA opt. + GGA energy calc. relative energies ΔE (kJ mol^{-1})
TS-1-Relax **1** + H_2O	0
TS-1(H_2O) **2**	−41
TS-1-Relax **1** + HOOH	0
TS-1(HOOH) **3**	−31
TS-1-Relax **1** + H_3N	0
TS-1(H_3N) **11**	−52

SCHEME 1

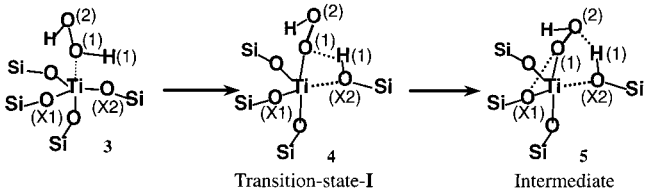

SCHEME 2

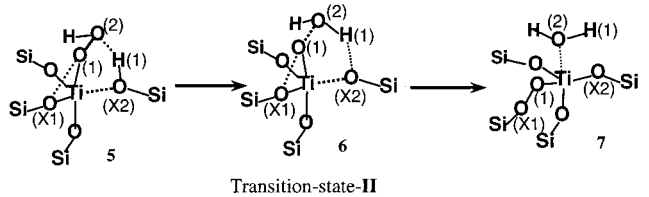

The relative energies for the reaction states, with respect to the energy sum of the initial separate reactants, TS-1-Relax and HOOH, are shown in Table 6. The energetic profile for activation of hydrogen peroxide over the TS-1 catalyst cluster model is shown in Figure 4. The geometry with atom names of the hydrated peroxo-TS-1 complex **7** is exhibited in Figure 5.

In Scheme 1, the hydrogen peroxide adsorbed TS-1 complex **3**, TS-1(HOOH), proceeded with the O(1)−H(1) bond cleavage, via transition-state-I **4**, to give the intermediate complex **5**, which was found to be located as a local minimum. An activation barrier for transformation from the TS-1(HOOH) complex **3** to the intermediate complex **5**, via the transition-state-I **4**, was calculated to be 69 kJ mol^{-1} as shown in Figure 4. The energy of the intermediate complex **5** was 11 kJ mol^{-1} relative to the energy of the initial separate reactants (TS-1-Relax + HOOH).

TABLE 6: Relative Energies for the Hydrogen Peroxide Activation Process[a]

Reaction States	LDA opt.+ GGA energy calc. Relative Energies (kJ mol^{-1})	
TS-1-Relax **1** + HOOH	0	
TS-1(HOOH) **3**	-31	**Scheme-1**
Transition-state-I **4**	38	
TS-1[(Ti)-OOH][HO-(Si)] **5**	11	**Scheme-2**
Transition-state-II **6**	69	
TS-1(Peroxo)(H_2O) **7**	-21	

[a] Peroxo = (Ti)-O-O-(Si).

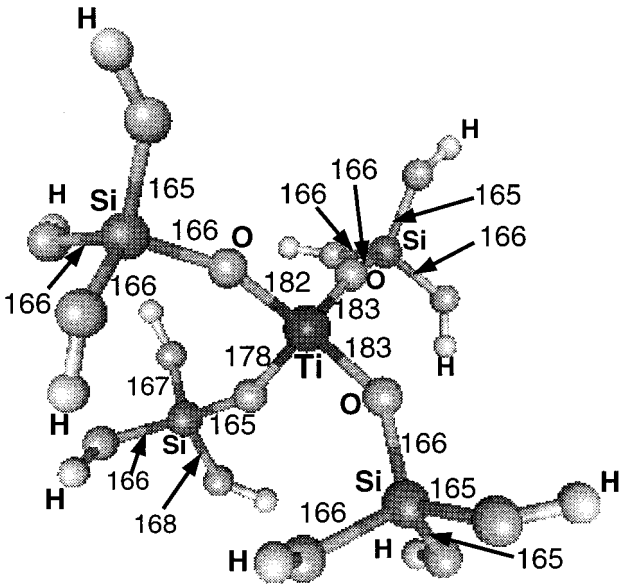

Figure 3. Relaxed geometry of the T1-site model for the TS-1 catalyst, optimized at LDA. All terminal hydrogen atoms were fixed at the initial coordinates to simulate the local crystal structure throughout geometry optimization.

The geometry of the transition-state-I **4** shows that the O(1)−H(1) distance is 184 pm and the O(X2)−H(1) distance is 101 pm, where the O(1)−H(1) bond is cleaved and the O(X2)−H(1) bond is formed. The Ti−O(X2) bond is elongated from 187 to 211 pm, and the hydrogen H(1) interacts with the oxygen O(2), its distance being 218 pm. The geometry of the intermediate complex **5**, TS-1[(Ti)−OOH][HO−(Si)], shows that the O(1)−H(1) distance is 204 pm and the O(X2)−H(1) distance is 105 pm. The Ti−O(1) distance is shortened to 192 pm, and the Ti−O(X2) distance is elongated to 214 pm. The hydrogen H(1) interacts with the oxygen O(2), and the H(1)−O(2) distance being 156 pm. This geometry of the intermediate complex **5** shows that the reacting atoms, O(1), O(2), O(X1), and Ti, are located almost on the same plane. Locations of these atoms facilitate the cleavage of the O(1)−O(2) bond and formation of the peroxo-bond, (Ti)−O(1)−O(X1)−(Si) in the TS-1 model complex. The hydrogen H(1) bonded to the oxygen O(X2) interacts with the oxygen O(2), which leads to produce H_2O with the transfer of the hydrogen H(1) to the oxygen O(2).

In Scheme 2, the intermediate complex **5**, TS-1-[(Ti)−OOH]-[HO−(Si)], transformed into the hydrated peroxo-TS-1 complex **7** via transition-state-II **6**. The O(1)−O(2) bond of the intermediate complex **5** was cleaved, and the oxygen O(1) was inserted into the Ti−O(X1) bond, to give the peroxo-moiety Ti−O(1)−O(X1)-Si of the hydrated peroxo-TS-1 complex **7**. An activation barrier for the transformation from the intermediate complex **5** to the hydrated peroxo-TS-1 complex **7**, via

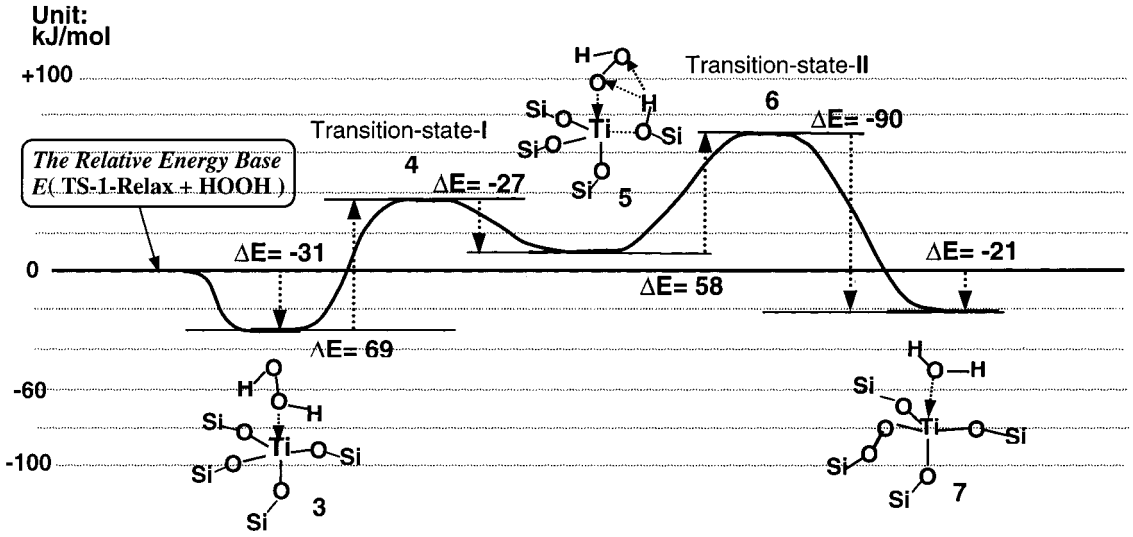

Figure 4. Energy profile for the reaction pathway for the activation of hydrogen peroxide over TS-1-Relax to form the hydrated-peroxo-TS-1 complex. The energy of the initial separate reactants (TS-1-Relax + HOOH) is taken as the reference base.

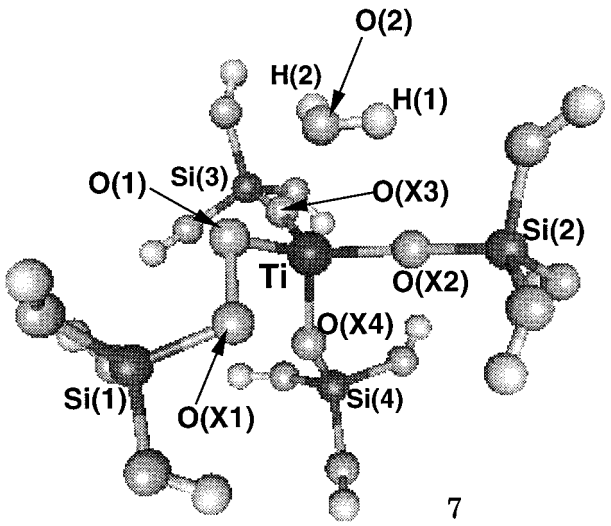

Figure 5. Geometry of the hydrated peroxo-TS-1 cluster model with atom names.

transition-state-II **6**, was calculated to be 58 kJ mol^{-1} as indicated in Figure 4. The energy for overall reaction from the initial separate reactants to the hydrated peroxo-TS-1 complex **7** was calculated to be −21 kJ mol^{-1} [TS-1-Relax **1** + HOOH → TS-1(Perox)(H_2O) **7**].

The geometry of the transition-state-II complex **6** shows that the O(1)−O(2) bond is elongated from 145 to 177 pm and that the O(1)−Ti bond is shortened from 192 to 189 pm, where the hydrogen H(1) is transferred to the oxygen O(2) to form a water molecule. The O(1)−O(X1) distance is shortened from 254 to 190 pm and the O(X1)−Ti bond is elongated from 186 to 194 pm. The hydrated peroxo-TS-1 complex **7** was obtained with insertion of the oxygen O(1) into the Ti−O(X1) bond. The geometry of the hydrated peroxo-TS-1 complex **7** shows that peroxo-related bond distances are 186 pm for Ti−O(1), 146 pm for O(1)−O(X1), and 169 pm for O(X1)−Si(1), where the distance between Ti and O(X1) is elongated to 247 pm.

Ethene Epoxidation with the Hydrated Peroxo-TS-1 Complex. The hydrated peroxo-TS-1 complex **7** derived by activation of hydrogen peroxide over the TS-1 catalyst model was proposed to be an active oxidizing agent in TS-1 catalyzed oxidation process. Using this hydrated peroxo-TS-1 complex **7** as an oxidizing agent, the ethene epoxidation mechanism was explored according to the postulated pathway as shown in Scheme 3.

SCHEME 3

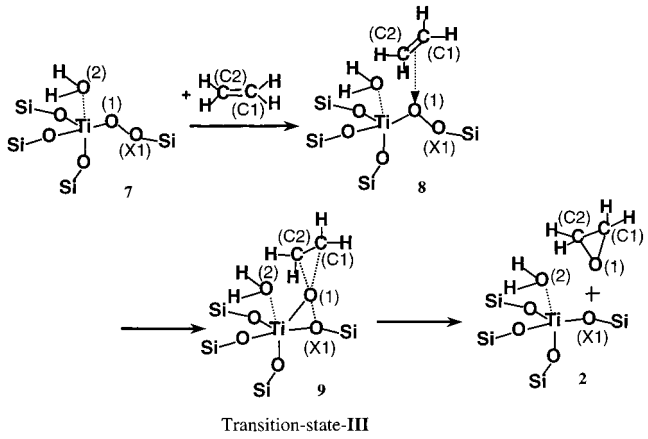

In Scheme 3, ethene interacted with the peroxo-oxygen O(1) of the hydrated peroxo-TS-1 complex **7**, to give the complex **8**, TS-1(peroxo)($H_2C{=}CH_2$)(H_2O), which transformed into ethylene epoxide and the water-adsorbed TS-1 complex **2**, via the transition-state-III complex **9**, with an energy barrier of 77 kJ mol^{-1} as shown in Figure 6. The overall reaction energy after desorption of ethylene epoxide and restoration of the TS-1(H_2O) complex **2** is −204 kJ mol^{-1}. [HOOH + $H_2C{=}CH_2$ → ethene epoxide + H_2O]. The reaction energy calculated from the standard enthalpies[51] of formation of the reactants, [HOOH + $H_2C{=}CH_2$], and the products, [ethylene epoxide + H_2O], is −208 kJ mol^{-1}. The overall reaction energy obtained above is in fairly good agreement with the experimental value, which has already been stated in the previous section.

The relative energies for the transition states, the intermediates, and the products with respect to the energy of the separate reactants, TS-1-Relax, HOOH, and $H_2C{=}CH_2$, are shown in Table 7. The energetic profile for ethene epoxidation with the hydrated peroxo-TS-1 complex is shown in Figure 6. The geometry of the transition-state-III complex **9** shows that the oxygen O(1) moved up toward ethene and is interacting with both ethene carbons, C(1) and C(2), the distances being 226 pm for O(1)−C(2) and 213 pm for O(1)−C(1), respectively. The Ti coordination distances to peroxo-oxygen atoms, O(1)

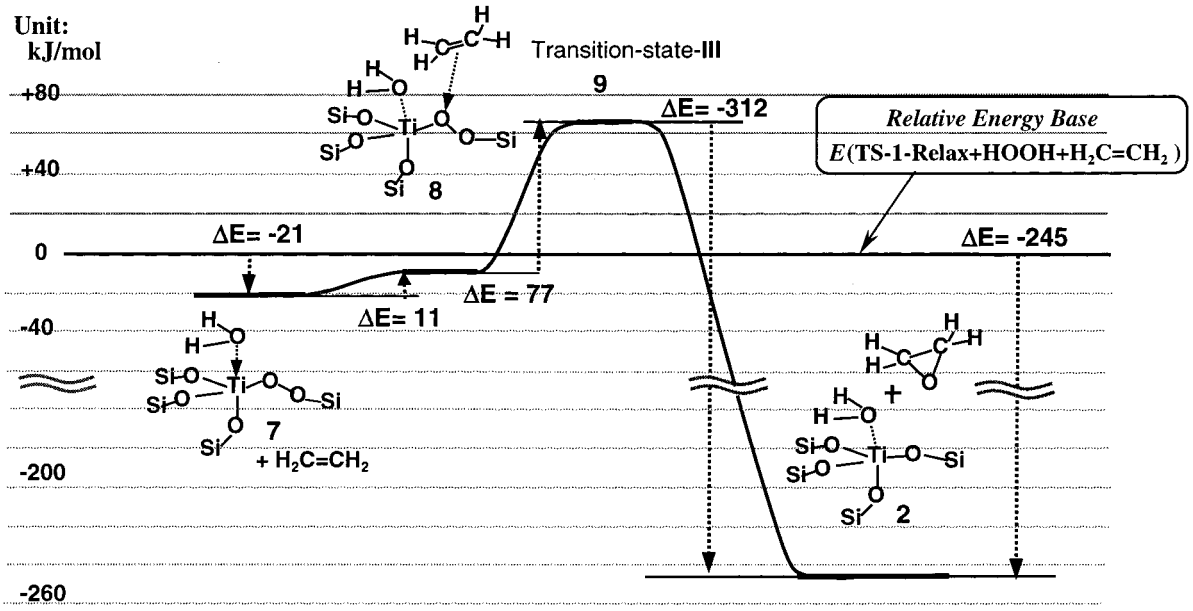

Figure 6. Energy profile for the reaction pathway for the ethene epoxidation, using the hydrated peroxo-TS-1 complex as an active oxidizing agent. The energy of the initial separate reactants (TS-1-Relax + HOOH + $H_2C{=}CH_2$) is taken as the reference base.

TABLE 7: Relative Energies of the Reaction Process for Ethene Epoxidation[a]

Reaction States	LDA opt.+ GGA energy calc. Relative Energies (kJ mol^{-1})	
TS-1-Relax **1** +HOOH + $H_2C{=}CH_2$	0	
TS-1(Peroxo)(H_2O) **7** + $H_2C{=}CH_2$	-21	
TS-1(Perox)($H_2C{=}CH_2$)(H_2O) **8**	-10	
Transition-state-III **9**	67	**Scheme-3**
TS-1(Epoxide) (H_2O) **10**	-244	
TS-1(H_2O) **2** + Epoxide	-245	
TS-1-Relax **1** + Epoxide + H_2O	-204	

[a] Epoxide = ethylene epoxide.

and O(X1), are 201 pm for both Ti−O(1) and Ti−O(X1), and the O(1)−O(X1) peroxo-bond is elongated to 168 pm. Ethene is approaching the oxygen O(1) in the direction of the extended line from the oxygen O(X1) to the oxygen O(1).

As indicated in Figure 7, transformation from the complex **8**, TS-1(peroxo)($H_2C{=}CH_2$)(H_2O), into the products, ethylene epoxide and the water-adsorbed TS-1 complex **2**, showed an activation barrier of 77 kJ mol^{-1} corresponding to the transition-state-III complex **9**. The activation height corresponding to the transition-state-III complex **9** was 67 kJ mol^{-1} with respect to the energy of the initial separate reactants.

Catalytic reaction cycle for ethene epoxidation over Titanosilicalite-1. On the basis of the current study, a catalytic epoxidation cycle is proposed with use of the peroxo-titanosilicalite-1 complex as an active oxidizing agent, as shown in Figure 8. Starting from the water-adsorbed TS-1 complex **1**, TS-1(H_2O), substitution of water with hydrogen peroxide gives the hydrogen peroxide TS-1 adduct **2**, TS-1(HOOH). Activation of hydrogen peroxide over the TS-1 catalyst model leads to form the hydrated peroxo-TS-1 species **7**, TS-1-(peroxo)(H_2O), via the intermediate complex **5**.

Using this TS-1(peroxo) species as an oxidizing agent, ethene epoxidation proceeds in the reaction pathway, where ethene attacks at the O(1) oxygen coordinated to the central titanium of the hydrated peroxo-TS-1 complex **7**, and leads to the formation of ethylene epoxide and the starting TS-1 complex **1**, TS-1(H_2O).

Catalytic Hydroxyamine Formation from Ammonia over Titanosilicalite-1. Ammoximation of ketones over the titano-

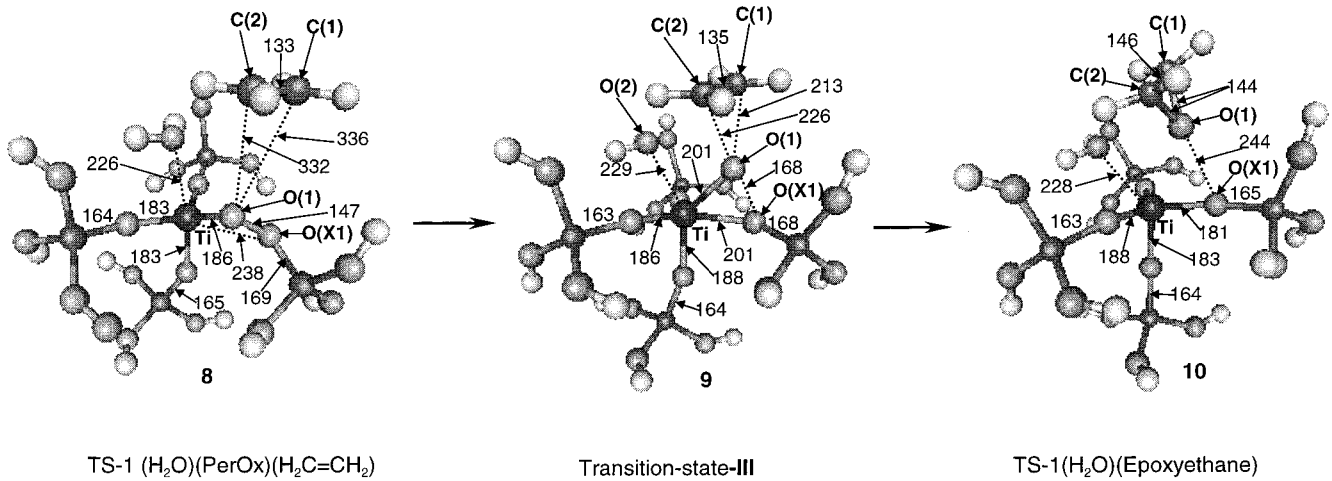

Figure 7. Reaction pathway of Scheme 3, with geometries of the ethene weakly bound hydrated peroxo-TS-1 complex **8**, the transition-state-III complex **9** and the ethene epoxide weakly bound TS-1 complex **10**.

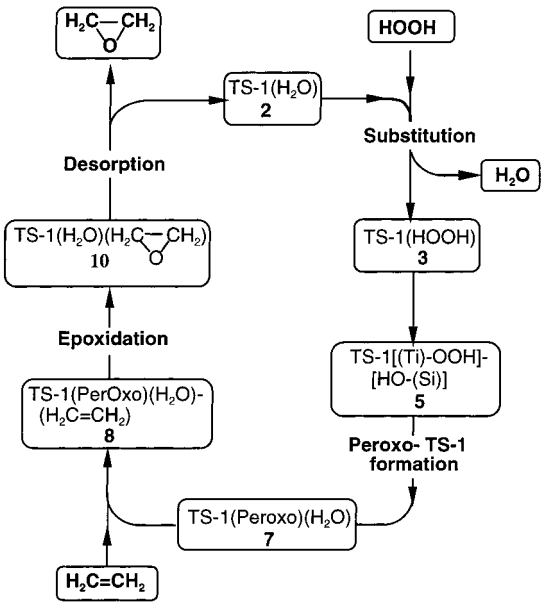

Figure 8. Catalytic ethene epoxidation cycle over the TS-1 catalyst in the presence of hydrogen peroxide.

SCHEME 4

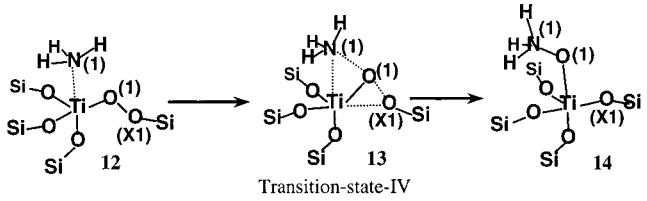

silicalite-1 (TS-1) catalyst in the presence of ammonia and hydrogen peroxide produced the corresponding oximes under mild conditions. It has been proposed that ammoximation proceeded via formation of an intermediate hydroxylamine derived from the catalytic oxidation of ammonia with hydrogen peroxide over the TS-1 catalyst. As described in the previous section, it was postulated that an activation of hydrogen peroxide over the TS-1 cluster model led to form the hydrated peroxo-TS-1 complex, containing a Ti-O-O-Si moiety, as an oxidizing agent. Using the hydrated peroxo-TS-1 complex as an oxidizing agent, the mechanism for hydroxylamine formation from ammonia was explored.

The adsorption energy of ammonia on the cluster model **1**, TS-1-Relax, was compared with those of water and hydrogen peroxide in Table 5. It showed adsorption energy of −52 kJ mol^{-1} relative to the energy of the initial separate system (TS-1-Relax + NH_3).

Interaction of ammonia with the hydrated peroxo-TS-1 complex **7** was examined and substitution of the water molecule of the hydrated peroxo-TS-1 complex **7** with ammonia resulted in an energy decrease of −14 kJ mol^{-1} to give the ammonia-adsorbed peroxo-TS-1 adduct **12**, TS-1(peroxo)(NH_3). The reaction mechanisms for oxidation of ammonia and successive formation of hydroxylamine were explored according to the postulated pathways, as shown in Schemes 4, 5, and 6.

Relative energies for the reactants in Schemes 4, 5, and 6, with respect to the energy of the initial separate reactants are given in Table 8. The energetic profile for the formation of hydroxylamine from ammonia, using the hydrated peroxo-TS-1 complex **7** as an oxidizing agent, is shown in Figure 9.

In Scheme 4, the ammonia-adsorbed peroxo-TS-1 adduct **12**, TS-1(peroxo)(NH_3), transformed to the (ammonia-*N*-oxide)-TS-1 complex **14**, TS-1(O−NH_3), where the adsorbed ammonia was oxidized by the peroxo-oxygen O(1) coordinated to the central Ti of the complex **12**. The activation barrier corresponding to the transition-state-IV complex **13**, was 56 kJ mol^{-1}, relative to the ammonia-adsorbed peroxo-TS-1 adduct **12**, TS-1(peroxo)(NH_3). The geometry of transition-state-IV indicated that the oxygen O(1) moved up toward ammonia and was interacting with the nitrogen N(1), the N(1)−O(1) distance being 200 pm. The peroxo-bond distance, O(1)−O(X1), was elongated to 171 pm and the distances between the central Ti, and the peroxo-oxygen atoms were 182 pm for Ti−O(1) and 212 pm for Ti−O(X1), respectively. The Ti−N(1) distance was elongated from 225 to 258 pm. The relative energy decrease of −87 kJ mol^{-1} was obtained for the transformation from the ammonia peroxo-TS-1-adduct **13**, TS-1(peroxo)(NH_3), into the (ammonia-*N*-oxide)TS-1 complex **14**, TS-1(O−NH_3).

In Scheme 5, the (ammonia-*N*-oxide)-TS-1 complex **14**, TS-1(−ONH_3), transformed into the (hydroxyl-amine)-TS-1-adduct-**A 16**, TS-1(H_2NOH)-**A**, with the hydrogen H(1) transfer from the nitrogen N(1) to the oxygen O(1) in the ammonia-*N*-

SCHEME 5

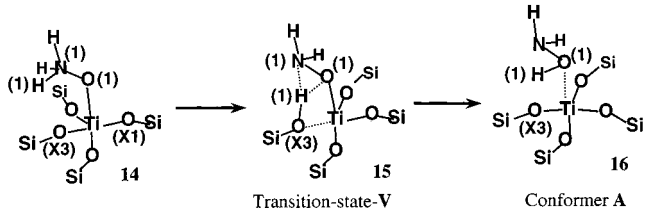

SCHEME 6

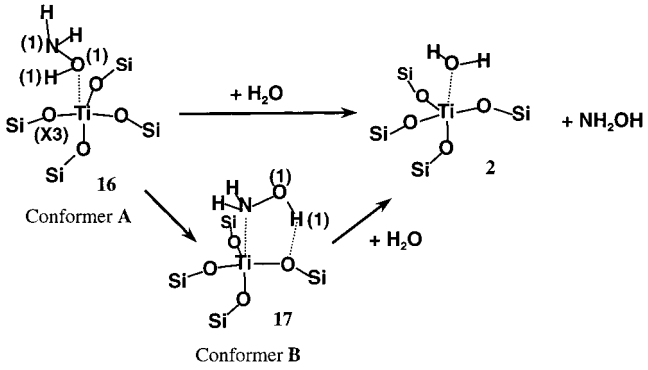

TABLE 8: Relative Energies for the Hydroxylamine Formation Process over the TS-1 Cluster Model[a]

Reaction States	LDA opt.+ GGA energy calc. Relative energies ΔE (kJ/mol)	
TS-1-Relax **1**+HOOH +H_3N	0	
TS-1(Peroxo)(H_2O) **7** + H_3N	-21	
TS-1(Peroxo)(H_3N) **12** + H_2O	-35	
Transition-state-IV **13** + H_2O	21	**Scheme-4**
TS-1(O-NH_3) **14** + H_2O	-122	
Transition-state-V **15** + H_2O	-61	**Scheme-5**
TS-1(H_2NOH)-A **16** + H_2O	-121	
TS-1(H_2NOH)-B **17** + H_2O	-156	**Scheme-6**
TS-1(H_2O) **2** + H_2NOH	-133	
TS-1-Relax **1** + H_2NOH + H_2O	-92	

[a] Peroxo = (Ti)-O-O-(Si).

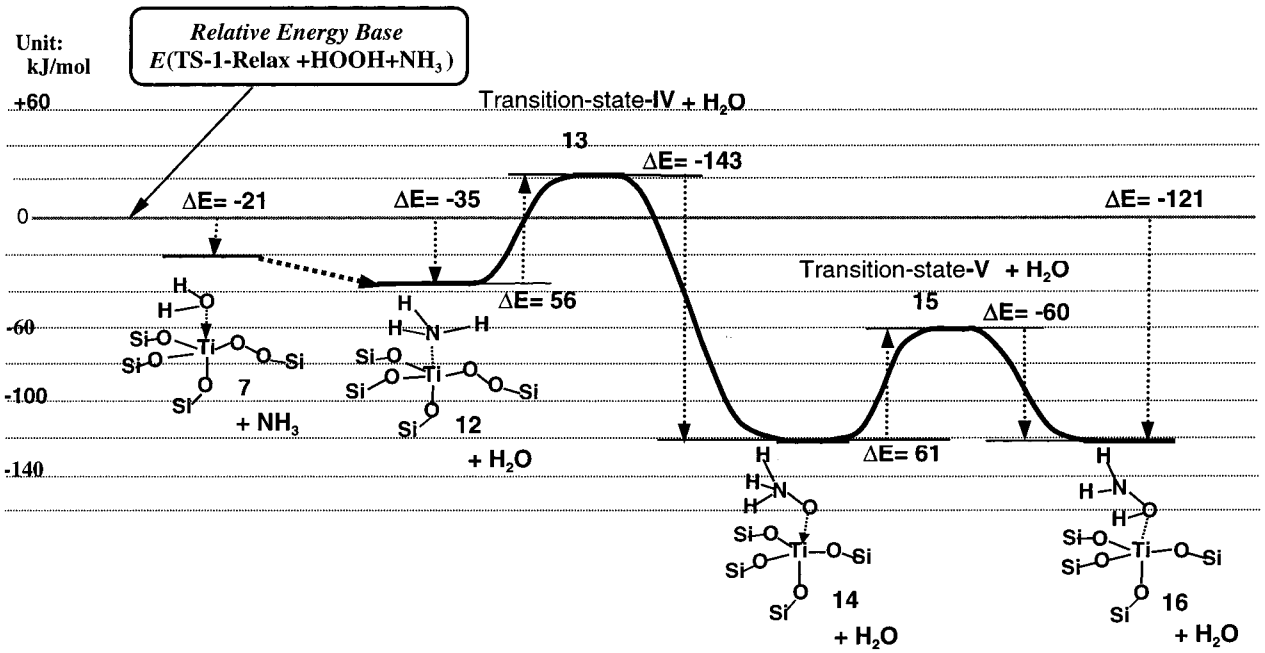

Figure 9. Energy profile for the reaction pathway for the ammonia oxidation to form hydroxylamine, using the peroxo-TS-1 complex as an active oxidizing agent. The energy of the initial separate reactants (TS-1-Relax + HOOH + NH_3) is taken as the reference base.

oxide moiety of the complex **14**, via transition-state-V **15**, with an activation barrier of 61 kJ mol^{-1}. The geometry of the transition-state-V complex **15** indicated that the hydrogen H(1) moved onto the oxygen O(X3), to form the O(X3)−H(1) bond, the distance being 104 pm, where the H(1)−N(1) bond distance was elongated from 105 to 211 pm and the Ti−O(X3) bond was elongated from 184 to 219 pm. The hydrogen H(1) of transition-state-V **15** was interacting with the oxygen O(1), the H(1)−O(1) distance being 156 pm. The hydrogen H(1) transfer in the transition-state-V complex **15** gave the (hydroxylamine)-TS-1-adduct-**A 16**, TS-1(H_2NOH)-**A**. In this reaction mechanism, the oxygen O(X3) played an important role in the process of transferring the hydrogen H(1) from the nitrogen N(1) to the oxygen O(1) of the (ammonia-*N*-oxide)-TS-1 **14**, to form the (hydroxylamine)-TS-1-adduct-**A 16**. The relative energy change for transformation from the (ammonia-*N*-oxide)TS-1 complex **14**, TS-1(ONH_3), to the (hydroxylamine)TS-1-adduct-**A 16**, TS-1(H_2NOH)-**A**, was 1 kJ mol^{-1}.

In Scheme 6, conformational change of the TS-1(H_2NOH)-**A 16** led to the TS-1(H_2NOH)-**B 17**, with an energy decrease of −35 kJ mol^{-1}. Substitution of the hydroxylamine molecule of TS-1(H_2NOH)-**A 16** with water reproduced the starting complex **2**, TS-1(H_2O) with a relative energy decrease of −12 kJ mol^{-1}. The overall reaction energy change for this catalytic reaction cycle is calculated to be −92 kJ mol^{-1} [HOOH + NH_3 → H_2NOH + H_2O].

Catalytic Cycle for Hydroxyamine Formation from Ammonia on Titanium Silicalite-1. On the basis of the current study, the catalytic reaction cycle for the formation of hydroxylamine from ammonia, using the peroxo-titano-silicalite-1 species as an active oxidizing agent, is proposed as shown in Figure 10. Starting from the water-adsorbed TS-1 complex **2**, TS-1(H_2O), substitution of water, with hydrogen peroxide gives the hydrogen peroxide TS-1 adduct **3**, TS-1(HOOH). The activation of hydrogen peroxide over the TS-1 catalyst model gives the hydrated peroxo-TS-1 species **7**, TS-1-(peroxo)(H_2O), as described in the previous section. Substitution of the water molecule adsorbed at the top of the central Ti atom in the hydrated peroxo-TS-1 species **7** with ammonia gives the ammonia-adsorbed peroxo-TS-1 adduct **12**, TS-1(peroxo)(NH_3).

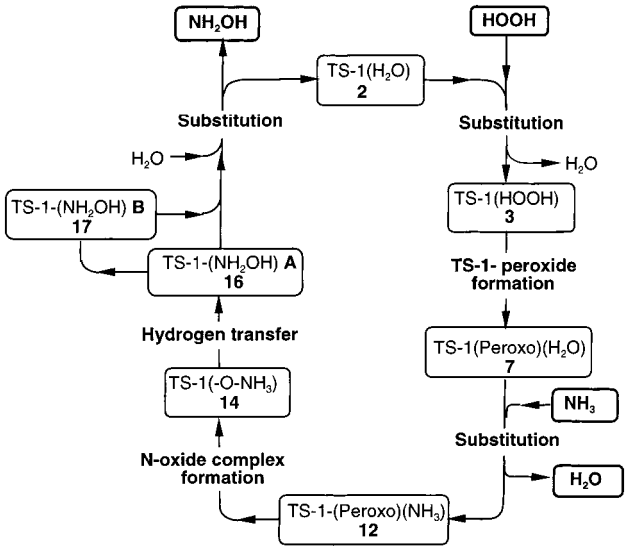

Figure 10. Catalytic reaction cycle for the ammonia oxidation to form hydroxylamine over the TS-1 catalyst in the presence of hydrogen peroxide.

The adduct **12** transforms to the ammonia-*N*-oxide TS-1 complex **14**, TS-1(−O−NH_3), which is derived from bond formation of the adsorbed ammonia N(1) with the peroxo-oxygen O(1) coordinated to the central Ti. The (ammonia-*N*-oxide)-TS-1 adduct **14**, TS-1(−O−NH_3), transforms into the (hydroxylamine)-TS-1 adduct-**A**, TS-1(H_2NOH)-**A**, **16** with the transfer of the hydrogen H(1) from the nitrogen N(1) to the oxygen O(1) in the ammonia-*N*-oxide moiety. The conformational change with the (hydroxylamine)-TS-1 adduct-**A**, TS-1(H_2NOH)-**A**, **16** gives the(hydroxylamine)-TS-1 adduct-**B**, TS-1(H_2NOH)-**B**, **17**. The desorption of H_2NOH from TS-1(H_2NOH)-**A** and -**B** by H_2O reproduces the starting complex **2**, TS-1(H_2O).

Conclusion

Density functional theory calculations were performed to study activation of hydrogen peroxide over the titano-silicalite

(TS-1) catalyst with the cluster model approximation. Energies of the complexes were evaluated by geometry optimization at the LDA level followed by GGA energy calculation. Results showed that possibility to form a peroxo-Ti species, containing the (Ti)-O-O-(Si) moiety, was revealed. The reaction mechanisms with this peroxo-Ti species as an oxidizing agent were explored in the postulated reaction pathways for the epoxidation of ethene and for the formation of hydroxylamine from ammonia, over the titano-silicalite (TS-1) catalyst.

In the activation of hydrogen peroxide over the TS-1 cluster model, the hydrogen peroxide-adsorbed TS-1 complex proceeded to form the intermediate complex, TS-1[(Ti)-OOH][HO-(Si)], with an activation barrier of 69 kJ mol^{-1} relative to the energy of TS-1(HOOH) complex. The intermediate complex, TS-1[(Ti)−OOH][HO−(Si)], was then transformed into the hydrated peroxo-TS-1 complex, containing a (Ti)-O-O-(Si) peroxo-moiety, with an activation barrier of 58 kJ mol^{-1} relative to the energy of the intermediate complex. Using the hydrated peroxo TS-1 complex, containing a (Ti)-O-O-(Si) peroxo-moiety, as an oxidizing agent, the epoxidation of ethene in the postulated reaction pathway proceeded to produce ethylene epoxide, with an activation barrier of 77 kJ mol^{-1} relative to the energy of the ethene weakly bound hydrated peroxo-TS-1 complex **8**.

For the process of the hydroxylamine formation from ammonia over the TS-1 catalyst, the following pathways using the hydrated peroxo TS-1 complex as an oxidizing agent are suggested. The water molecule of the hydrated peroxo-TS-1 complex is substituted with ammonia to give the ammonia-adsorbed peroxo-TS-1 complex. The ammonia-adsorbed peroxo-TS-1 complex is transformed into the ammonia-*N*-oxide TS-1 complex, with an activation barrier of 56 kJ mol^{-1} relative to the energy of the ammonia-adsorbed peroxo-TS-1 complex. The (ammonia-*N*-oxide)-TS-1 complex was transformed into the (hydroxylamine)-TS-1 complex, with the hydrogen transfer from the nitrogen to the oxygen in the ammonia-*N*-oxide moiety, with an activation barrier of 61 kJ mol^{-1}, relative to the energy of the (ammonia-*N*-oxide)-TS-1 complex.

The DFT calculation results exhibited the possibility to form the peroxo-TS-1 complex, containing the (Ti)-O-O-(Si) moiety, as an active oxidizing agent, in the activation of hydrogen peroxide over the TS-1 catalyst. Using the peroxo-TS-1 complex as an active oxidizing agent, catalytic cycles for the epoxidation of ethene and for the formation of hydroxylamine from ammonia over the TS-1 catalyst in the presence of hydrogen peroxide are proposed.

Acknowledgment. The authors express their sincere thanks to Prof. A. Imamura, Hiroshima Kokusai Gakuin University, for his helpful and stimulating discussion.

References and Notes

(1) Murugavel, R.; Roesky, H. W. *Angew. Chem., Int. Ed. Engl.* **1997**, *36*, 477.
(2) Nottari, B. *Adv. Catal.* **1996**, *41*, 253.
(3) Meier, W. M.; Olsen, D. H. *Atlas of Zeolite Structure Types*, Butterworths, 1987.
(4) Taramasso, T.; Perego, G.; Notari, B. U.S. Patent 4,410,501, 1983.
(5) van der Pol, A. J. H. P.; van Hooff, J. H. C. *Appl. Catal.* **1992**, *A 92*, 93.
(6) Reddy, J. S.; Kumar, R. *J. Catal.* **1991**, *130*, 440.
(7) Serano, D. P.; Li, Hong-X.; Davis, M. E. *J. Chem. Soc., Chem. Commun.* **1992**, 745.
(8) Camblor, M. H.; Corma, A.; Perez Pariente, J. *J. Chem. Soc. Chem. Commun.* **1992**, 589.
(9) Corma, A.; Camblor, M. A.; Esteve P.; Martinez, A.; Perez Pariente, J. *J. Catal.* **1994**, *145*, 151.
(10) Tuel, A. *Zeolites* **1995**, *15*, 236.
(11) Corma, A.; Navaro, M. T.; Perez-Pariente, J. *J. Chem. Soc., Chem. Commun.* **1994**, 147.
(12) Blasco, A. T.; Corma, A.; Navaro, M. T.; Perez-Pariente, J. *J. Catal.* **1995**, *156*, 65.
(13) Clelici, M. G.; Bellussi, G.; Romano, U. *J. Catal.* **1991**, *129*, 1.
(14) Clelici, M. G.; Bellussi, G.; Romano, U. *J. Catal.* **1991**, *129*, 159.
(15) Bellussi, G.; Carati, A.; Clelici, M. G.; Madinelli, G.; Millini, R. *J. Catal.* **1992**, *133*, 220.
(16) Clelici, M. G.; Ingallina, P. *J. Catal.* **1993**, *140*, 71.
(17) Khouw, C. B.; Dartt, C. B.; Labinger, J. A.; Davis, M. E. *J. Catal.* **1994**, *149*, 195.
(18) Tatsumi, T.; Nakamura, M.; Negishi, S.; Tominaga, T. *J. Chem. Soc., Chem. Commun.* **1990**, 476.
(19) Bellussi, G.; Rigutto, M. S. *Stud. Surf. Sci. Catal.* **1994**, *85*, 177.
(20) Gontier, S.; Tuel, A. *J. Catal.* **1995**, *157*, 124.
(21) Tuel, A.; Moussa-Khouzami, S.; Taarit, Y. B.; Naccache, C. *J. Mol. Catal.* **1991,** *68*, 45.
(22) Tangaraj, A.; Kumar, R.; Mirajkar, S. P.; Ratnasamy, P. *J. Catal.* **1991**, *130*, 1.
(23) Thangaraj, A.; Sivasanker, S.; Ratnasamy, P. *J. Catal.* **1991**, *131*, 394.
(24) Zecchima, A.; Spoto, G.; Bordiga, S.; Geobaldo, F.; Petrini, G.; Leofanti, G.; Padovan, M.; Mantegazza, M.; Roffia, P. *Stud. Surf. Sci. Catal.* **1993**, *75*, 719.
(25) Mantegazza, M. A.; Leofanti, G.; Petrini, G.; Padvan M.; Zecchima, A.; Bordiga, S. *Stud. Surf. Sci. Catal.* **1994**, *82*, 541.
(26) Wu, P.; Komatsu, T.; Yashima, T. *J. Catal.* **1997**, *168*, 400.
(27) Sudhakar Reddy, J.; Sivasanker, S.; Ratnasamy, P. *J. Mol. Catal.* **1991**, *69*, 383.
(28) Blasco, T.; Camblor, M. A.; Corma, A.; Perez-Pariente, J. *J. Am. Chem. Soc.* **1993**, *115*, 11806.
(29) Bellussi, G.; Fatore, V. *Stud. Surf. Sci. Catal.* **1991**, *69*, 79.
(30) Pei, S.; Zajak, G. W.; Kaduck, J. A.; Faber, J.; Boyanov, B. I.; Duck, D.; Fazzini, D.; Morrison, T. I.; Yang, D. S. *Catal. Lett.* **1993**, *21*, 333.
(31) Bordiga, S.; Collucia, S.; Lamberti, C.; Marchese, Zecchina, L.; A.; Boscherini, F.; Buff, F.; Genoni, F.; Leofanti, G.; Petrini, G.; Vlaic, G. *J. Phys. Chem.* **1994**, *98*, 4125.
(32) Davis, R. J.; Liu, Z.; Tabora, J. E.; Wielband, W. S. *Catal. Lett.* **1995**, *34*, 101.
(33) Earley, C. W. *Inorg. Chem.* **1992**, *31*, 1250.
(34) Feher, F. J.; Newman, D. A.; Walzner, J. F. *J. Am. Chem. Soc.* **1989**, *111*, 1741.
(35) Duprey, E.; Beaunier, P.; Springuel-Huet, M. A.; Bozon-Verduraz, F.; Fraissard, J.; Manoli, J. M.; Brégeault, J. M. *J. Catal.* **1997**, *165*, 22.
(36) Zecchima, A.; Bordiga, S.; Lamberti, C.; Ricchiardi, G.; Scaranto, D.; Petrini, G.; Leofanti, G.; Mantegazza, M. *Catal. Today* **1996**, *32*, 97.
(37) Karlsen, E.; Schöffel, K. *Catal. Today* **1996**, *32*, 107.
(38) Neurock, M.; Manzer, L. E. *Chem. Commun.* **1996**, 1133.
(39) Vayssilov, G. N.; van Santen, Rutger A. *J. Catal.* **1998**, *175*, 170.
(40) Sinclair, P. E.; Catlow, C. R. A. *Chem. Commun.* **1997**, 1881.
(41) Sinclair, P. E.; Catlow, C. R. A. *J. Phys. Chem. B* **1999**, *103*, 1084.
(42) Munakata, H.; Oumi, Y.; Miyamoto, A. *Stud. Surf. Sci. Catal.* **1998**, 227.
(43) Molecular Simulations Inc. *DMol*, version 960.
(44) Baker, J. *J. Comput. Chem.* **1986**, *7*, 385.
(45) Baker, J. *J. Comput. Chem.* **1992**, *13*, 240.
(46) Becke, A. D. *Phys. Rev. A* **1988**, *38*, 3098.
(47) Perdew, J. P. in *Electronic Structure of Solids*; Ziesche P.; Eschering H., Eds.; Akademic Verlag: Berlin, Germany, 1991.
(48) *InsightII*, version 980, Molecular Simulations Inc., Sandiego, 1999.
(49) *WebLabViewerLite*, version 3.10, Molecular Simulations Inc., San Diego, 1998.
(50) Jentys, A.; Catlow, R. A. *Catal. Lett.* **1993**, *22*, 251.
(51) Milini, R.; Perego, G.; Seiti, K. *Stud. Surf. Sci. Catal.* **1994**, *84*, 2123.
(52) Oumi, T.; Matsuba, K.; Kubo, M.; Inui, T.; Miyamoto, A. *Microporous Matter* **1995**, *4*, 5.
(53) Sutton, L. E., Ed. *Tables of Interatomic Distances and Configuration in Molecule and Ions*; The Chemical Society, Special Publication No. 11, 1958.
(54) David, R. L., Ed. *CRC Handbook of Chemistry and Physics*; 79th ed., CRC Press, 1998−1999.
(55) Olson, D. H.; Kokotallo, G. T.; Lawton, S. L. *J. Phys. Chem.* **1981**, *85*, 2238.